Science Translational Medicine
AAAS

Increased in Vivo Amyloid-β42 Production, Exchange, and Loss in Presenilin Mutation Carriers

Rachel Potter *et al.*

Sci Transl Med **5**, 189ra77 (2013);
DOI: 10.1126/scitranslmed.3005615

Editor's Summary

Aβ42: A Cycle of Gain and Loss

The amyloid hypothesis of Alzheimer's disease (AD) proposes that increased production or impaired clearance of A β42 peptide causes deposition of amyloid in plaques, nerve destruction, and ultimately AD dementia. Animal model studies based on human autosomal dominant mutations have shown that increasing the production of A β peptides, especially A β42, can recapitulate amyloidosis. Potter *et al.* have now used a stable isotope labeling kinetics (SILK) approach to measure A β isoform kinetics to test specific hypotheses regarding the production rates of the Aβ 38, Aβ40, and Aβ42 peptides in individuals carrying autosomal dominant AD mutations and related noncarriers. The authors found an increased A β42 production rate in AD mutation carriers that was ~25% higher than that in noncarriers. In addition to increased production rates, the authors unexpectedly found altered A β42 kinetics in mutation carriers that indicated both a reversible exchange pool and increased irreversible loss. Future studies could quantify the effects of proposed disease-modifying drugs to normalize altered Aβ kinetics and provide a metric to gauge target engagement for therapeutic trials.

Science Translational Medicine (print ISSN 1946-6234; online ISSN 1946-6242) is published weekly, except the last week in December, by the American Association for the Advancement of Science, 1200 New York Avenue NW, Washington, DC 20005.

ALZHEIMER'S DISEASE

Increased in Vivo Amyloid-β42 Production, Exchange, and Loss in Presenilin Mutation Carriers

Rachel Potter,[1]* Bruce W. Patterson,[2]* Donald L. Elbert,[3] Vitaliy Ovod,[1] Tom Kasten,[1] Wendy Sigurdson,[1,4] Kwasi Mawuenyega,[1] Tyler Blazey,[4,5] Alison Goate,[4,6,7] Robert Chott,[2] Kevin E. Yarasheski,[2] David M. Holtzman,[1,4,6] John C. Morris,[1,4,6] Tammie L. S. Benzinger,[4,5,8] Randall J. Bateman[1,4,6†]

Alzheimer's disease (AD) is hypothesized to be caused by an overproduction or reduced clearance of amyloid-β (Aβ) peptide. Autosomal dominant AD (ADAD) caused by mutations in the presenilin (*PSEN*) gene have been postulated to result from increased production of Aβ42 compared to Aβ40 in the central nervous system (CNS). This has been demonstrated in rodent models of ADAD but not in human mutation carriers. We used compartmental modeling of stable isotope labeling kinetic (SILK) studies in human carriers of *PSEN* mutations and related noncarriers to evaluate the pathophysiological effects of *PSEN1* and *PSEN2* mutations on the production and turnover of Aβ isoforms. We compared these findings by mutation status and amount of fibrillar amyloid deposition as measured by positron emission tomography (PET) using the amyloid tracer Pittsburgh compound B (PIB). CNS Aβ42 to Aβ40 production rates were 24% higher in mutation carriers compared to noncarriers, and this was independent of fibrillar amyloid deposits quantified by PET PIB imaging. The fractional turnover rate of soluble Aβ42 relative to Aβ40 was 65% faster in mutation carriers and correlated with amyloid deposition, consistent with increased deposition of Aβ42 into plaques, leading to reduced recovery of Aβ42 in cerebrospinal fluid (CSF). Reversible exchange of Aβ42 peptides with preexisting unlabeled peptide was observed in the presence of plaques. These findings support the hypothesis that Aβ42 is overproduced in the CNS of humans with *PSEN* mutations that cause AD, and demonstrate that soluble Aβ42 turnover and exchange processes are altered in the presence of amyloid plaques, causing a reduction in Aβ42 concentrations in the CSF.

INTRODUCTION

The pathogenic causes of Alzheimer's disease (AD) are not fully understood, partly due to the difficulty in demonstrating the steps that lead to dementia in humans. However, rare autosomal dominant AD (ADAD) can be predicted with nearly 100% certainty in individuals with specific mutations in the genes encoding presenilin 1 (*PSEN1*), presenilin 2 (*PSEN2*), or the amyloid precursor protein (APP) (*1*). Recent findings suggest that a series of pathophysiological changes occur in the brains of ADAD mutation carriers decades before clinical dementia manifests (*2*). The amyloid hypothesis (*3*) predicts that AD is caused by increased production or decreased clearance of amyloid-β (Aβ) in the brain, resulting in amyloidosis and a pathological hallmark of AD, amyloid plaques. Aβ is produced from the C-terminal fragment of APP by cleavage of APP by β-secretase to form C99, followed by cleavage of C99 by *PSEN1* or *PSEN2*, the enzymatic components of γ-secretase (*4*). The principal peptide produced by γ-secretase is a 40–amino acid peptide (Aβ40), but this enzymatic cleavage lacks specificity and peptides ranging in length from 38 to 43 amino acids are produced (*5*). Aβ42 has attracted considerable attention because it has greater amyloidogenic properties and is the principal component of amyloid plaques (*6*). In support of the amyloid hypothesis, an APP mutation that reduces Aβ production is associated with a strong protective effect against AD (*7*), whereas duplication of *APP* or mutations that are thought to increase total Aβ species or Aβ42 relative to Aβ40 cause dominantly inherited AD (*8*–*10*). In cell culture and in plasma from human ADAD participants, *PSEN* mutations have been reported to increase the Aβ42/Aβ40 ratio (*11*–*14*), which is hypothesized to increase the risk of amyloidosis (*15*). However, others have found that neither the Aβ42/Aβ40 ratio nor Aβ42 concentrations are increased in vitro (*16*). Furthermore, findings of reduced Aβ42 concentrations in the cerebrospinal fluid (CSF) of ADAD participants (*13*, *17*) do not directly support the hypothesis that increased Aβ42 production is an etiological mechanism in dominantly inherited AD.

We previously used stable isotope labeling kinetics (SILK) to examine the turnover kinetics of Aβ in sporadic late-onset AD (*18*). Both sporadic AD and ADAD are associated with lower CSF Aβ42 concentrations and Aβ42/Aβ40 ratios (*13*, *17*, *19*–*21*). However, *PSEN* mutations in ADAD are hypothesized to cause increased Aβ42 production (*4*, *12*, *22*), although direct evidence for increased in vivo production of Aβ42 in humans has not been reported.

We hypothesized that the central nervous system (CNS) Aβ42/Aβ40 production rate ratio is increased in *PSEN1* and *PSEN2* mutation carriers compared to noncarriers. To address this hypothesis, we performed in vivo SILK studies in participants with ADAD mutations and sibling noncarrier controls. A comprehensive compartmental model was

[1]Department of Neurology, Washington University School of Medicine, 660 South Euclid Avenue, St. Louis, MO 63110, USA. [2]Department of Medicine, Washington University School of Medicine, St. Louis, MO 63110, USA. [3]Department of Biomedical Engineering, Washington University in St. Louis, One Brookings Drive, St. Louis, MO 63130, USA. [4]Knight Alzheimer's Disease Research Center, Washington University School of Medicine, St. Louis, MO 63110, USA. [5]Department of Radiology, Washington University School of Medicine, St. Louis, MO 63110, USA. [6]Hope Center for Neurological Disorders, Washington University School of Medicine, St. Louis, MO 63110, USA. [7]Department of Psychiatry, Washington University School of Medicine, St. Louis, MO 63110, USA. [8]Department of Neurological Surgery, Washington University School of Medicine, St. Louis, MO 63110, USA.
*These authors contributed equally to this work.
†Corresponding author. E-mail: batemanr@wustl.edu

developed to determine steady-state metabolic kinetic parameters including fractional turnover rates (FTRs) and production rates of Aβ38, Aβ40, and Aβ42 for each participant. The Aβ kinetic parameters were compared to the presence of a *PSEN* mutation and insoluble amyloid deposition, which was measured by positron emission tomography (PET) imaging of Pittsburgh compound B (PIB).

RESULTS

SILK was performed in 11 individuals who carry mutations in *PSEN* associated with ADAD and in 12 sibling control persons who do not carry *PSEN* mutations. PIB-PET imaging (*23*) showed virtually no detectable amyloidosis in all noncarriers and in four of the mutation

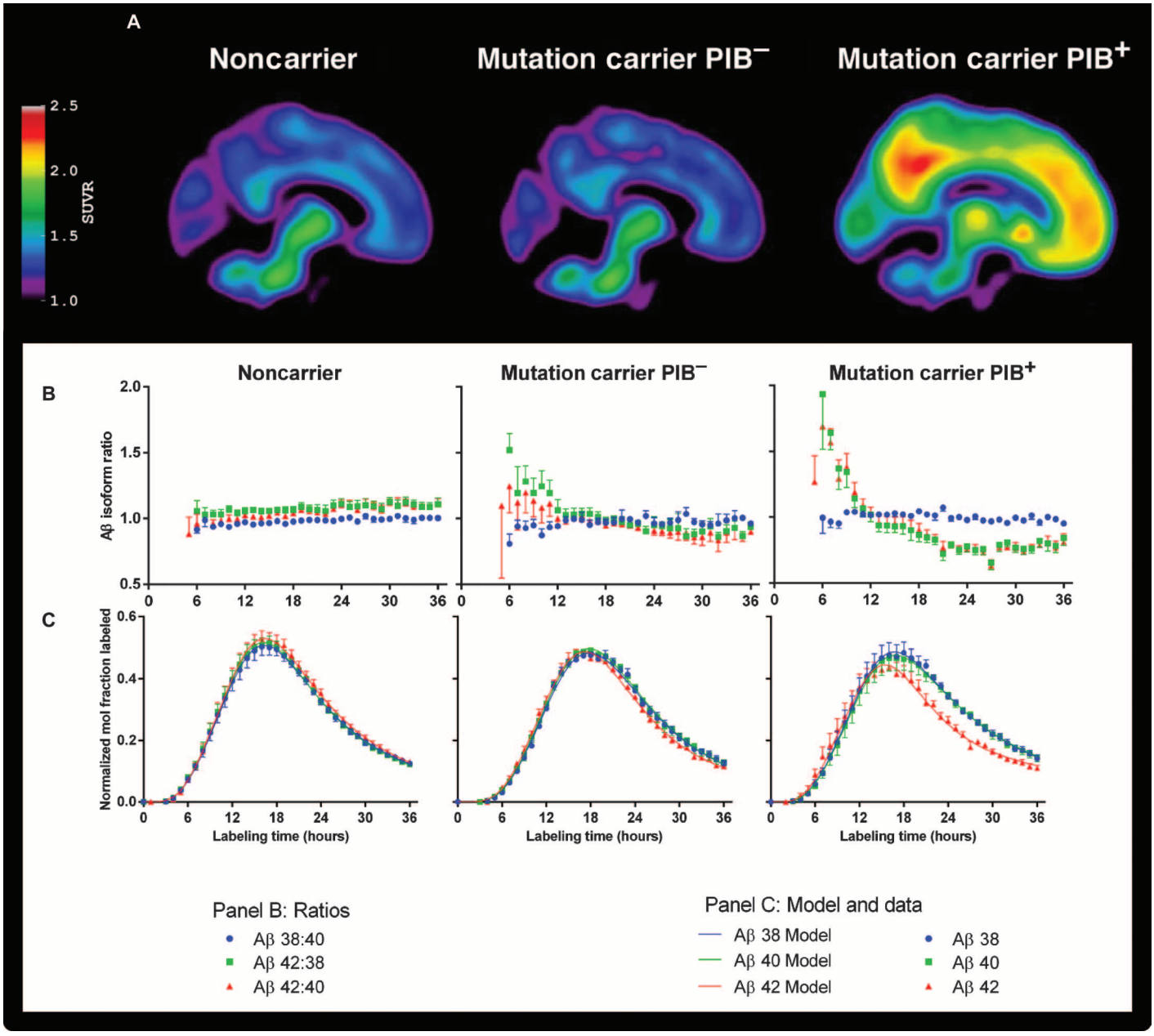

Fig. 1. PET images and isotopic enrichment time course profiles of CSF Aβ peptides. (**A**) Composite PET images showing [^{11}C]PIB binding in participants who are noncarriers of *PSEN* mutations (left column), and *PSEN* mutation carriers who lack (PIB$^-$, middle column) or have (PIB$^+$, right column) evidence of amyloidosis. (**B** and **C**) Average Aβ isotopic kinetic time course profiles in CSF showing the Aβ42/Aβ40, Aβ38/40, and Aβ42/Aβ38 isotopic enrichment ratios [B, middle panel: Aβ38/40 (blue circles), Aβ42/Aβ38 (green squares), and Aβ42/Aβ40 (red triangles)] and as enrichment ratios normalized to plasma leucine plateau enrichments [C, lower panel: Aβ38 (blue circles), Aβ40 (green squares), and Aβ42 (red triangles)]. Aβ38 and Aβ40 present similar labeling profiles in all subject groups, whereas Aβ42 kinetics deviate from Aβ38 and Aβ40 only in mutation carriers, as evident in the Aβ42/Aβ40 and Aβ42/Aβ38 ratio profiles. Data points represent the means ± SD for group-averaged values, and the solid lines represent the model fits to the data using the model in Fig. 2.

carriers (denoted PIB$^-$), and considerable amyloidosis in seven mutation carriers (denoted PIB$^+$) (Fig. 1A). A mean cortical binding potential (MCBP) score was calculated from the PET images to obtain a continuous quantitative covariate for statistical analyses.

Differential Aβ isoform kinetics by mutation and amyloid deposition

Plasma leucine enrichment approximated a constant plateau during the 9-hour intravenous $^{13}C_6$-leucine infusion, and then rapidly decreased after the infusion was stopped (fig. S1). The $^{13}C_6$-leucine isotopic enrichments of Aβ38, Aβ40, and Aβ42 recovered from CSF were compared between mutation carriers, with or without amyloidosis, and noncarriers to address the relationship between Aβ isoform metabolic kinetics, mutation status, and amyloid deposition.

To compare Aβ isoform kinetics, we plotted ratios of labeled Aβ isoform enrichments in the CSF so that a ratio of 1 indicates the same isotopic enrichment and kinetics between Aβ isoforms. The Aβ38/Aβ40 labeling ratio was about 1 from 5 to 36 hours in all participant groups (Fig. 1B, no significant group by time interaction), indicating similar kinetics between Aβ38 and Aβ40. Similarly, the Aβ42/Aβ40 and Aβ42/Aβ38 labeling ratios were nearly constant at 1 over time in noncarriers. However, in mutation carriers, the Aβ42/Aβ40 and Aβ42/Aβ38 labeling ratios were elevated during early time points and decreased at later time points (Fig. 1B) in relation to plaque status. Repeated-measures analysis of variance (ANOVA) revealed a significant group by time interaction for both the Aβ42/Aβ40 and Aβ42/Aβ38 labeling ratios ($P < 0.0001$), with a significant linear contrast ($P < 0.01$) between groups at ≤9 hours and at ≥18 hours, showing an increasing magnitude of effect (noncarrier < mutation carrier PIB$^-$ < mutation carrier PIB$^+$). The Aβ isoform enrichment mismatch was more pronounced in participants with amyloid deposition (PIB$^+$), caused by an earlier and lower Aβ42 peak with a flatter terminal tail compared to Aβ38 and Aβ40 (Fig. 1C). The time to reach peak ^{13}C labeling in each Aβ isoform was measured for each participant. The Aβ38/Aβ40 peak time ratio was not different between mutation carrier and noncarrier groups (1.01 ± 0.01 versus 1.00 ± 0.01, respectively). In contrast, Aβ42 peaked at the same time as did Aβ40 in the noncarrier group (Aβ42/Aβ40 peak time ratio = 1.01 ± 0.03), whereas Aβ42 peaked significantly earlier than did Aβ40 in the mutation group (peak time ratio = 0.93 ± 0.05; $P = 0.015$, for mutation effect; $P < 0.001$, for PIB MCBP score).

A multicompartment model to describe Aβ isoform kinetics

A comprehensive compartmental model was developed to quantify steady-state Aβ isoform kinetic parameters for each participant data set. The model incorporated the plasma leucine, Aβ enrichment time course profiles, and the CSF Aβ isoform concentrations for each subject (schematically depicted in Fig. 2). Figures S2 to S5 show curve fits for each Aβ isoform time course for each participant. A reversible exchange compartment was necessary to fit the sigmoidal decay of many labeling curves, especially Aβ42 in PIB$^+$ participants. The model included an

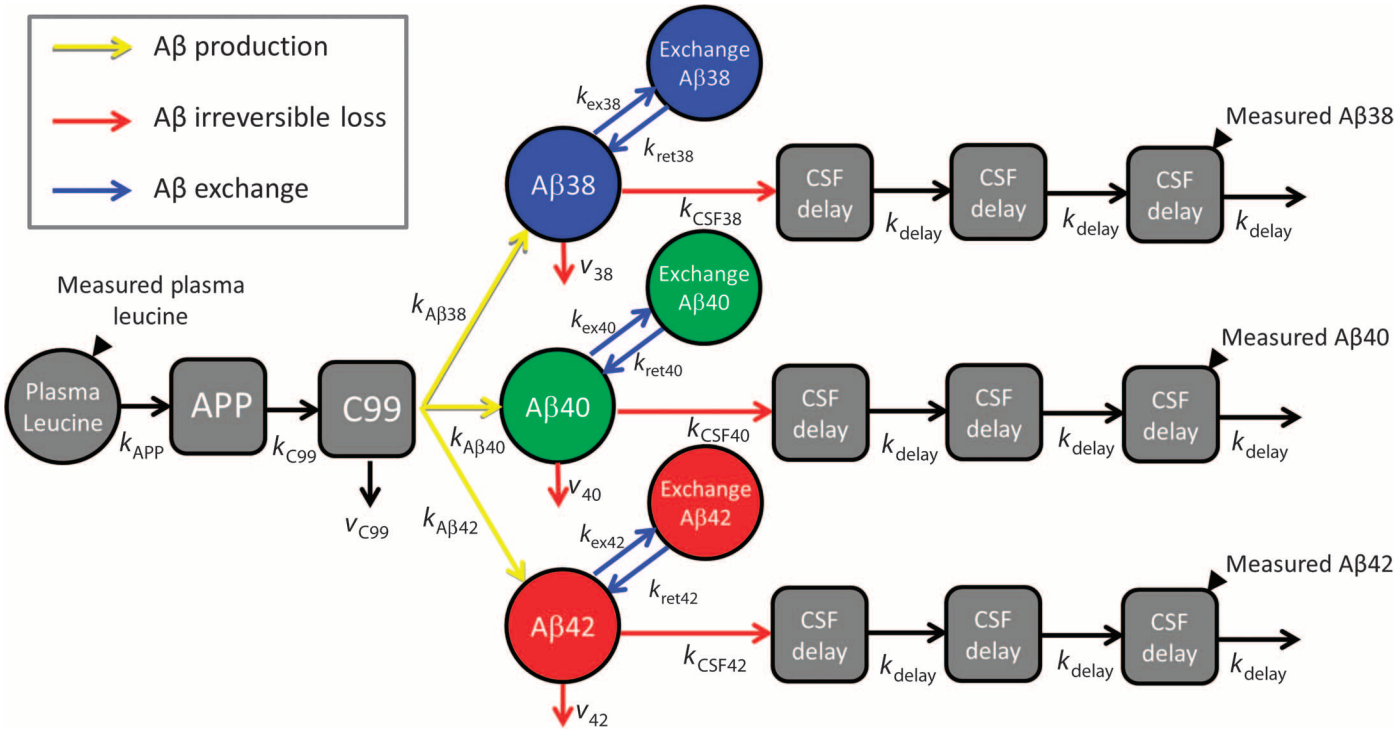

Fig. 2. Schematic diagram of compartmental model of Aβ38, Aβ40, and Aβ42 metabolism. Small solid black triangles depict sampling sites for plasma leucine and CSF Aβ peptides. Production of Aβ peptides is signified by yellow arrows, exchange by blue arrows, and irreversible loss by red arrows. The model incorporated the labeling time course of plasma $^{13}C_6$-leucine, APP production and processing to C99 peptide, and Aβ38, Aβ40, or Aβ42 production from C99. The labeled Aβ38, Aβ40, and Aβ42 that are sampled in CSF are presumed to be soluble within the "brain" compartment. The soluble Aβ peptides may exchange with other unlabeled Aβ structures, may be transported to CSF, or may be lost because of other processes (for example, transport to blood, plaque deposition, or cellular degradation). Transport through CSF is modeled as a three-compartment time delay.

Table 1. Complete list of model parameters. All units are first-order rate constants with units of pools/hour, except for scaling factors (SFs), which are unitless, and k_{APP}, which is a zero-order rate constant for APP production (ng/hour). Note that $k_{C99} = k_{delay}$; $k_{A\beta38} + k_{A\beta40} + k_{A\beta42} = v_{C99}$; and $k_{A\beta38} + k_{A\beta40} + k_{A\beta42} + v_{C99} = k_{delay}$. Values are means ± SD.

Parameter	Noncarriers	Mutation carrier PIB$^-$	Mutation carrier PIB$^+$
k_{APP}	1171 ± 227	1304 ± 602	1291 ± 324
k_{C99}	0.666 ± 0.112	0.553 ± 0.083	0.695 ± 0.096
$k_{A\beta38}$	0.062 ± 0.010	0.055 ± 0.016	0.059 ± 0.008
$k_{A\beta40}$	0.238 ± 0.041	0.187 ± 0.023	0.247 ± 0.037
$k_{A\beta42}$	0.033 ± 0.006	0.034 ± 0.007	0.041 ± 0.006
v_{C99}	0.333 ± 0.056	0.276 ± 0.041	0.347 ± 0.048
v_{38}	0.069 ± 0.023	0.075 ± 0.027	0.054 ± 0.015
v_{40}	0.074 ± 0.023	0.082 ± 0.037	0.050 ± 0.013
v_{42}	0.064 ± 0.014	0.126 ± 0.072	0.120 ± 0.037
k_{CSF}	0.074 ± 0.023	0.082 ± 0.037	0.050 ± 0.013
k_{ex38}	0.020 ± 0.038	0.000 ± 0.000	0.000 ± 0.000
k_{ex40}	0.016 ± 0.032	0.009 ± 0.018	0.000 ± 0.000
k_{ex42}	0.010 ± 0.021	0.041 ± 0.045	0.120 ± 0.107
k_{ret}	0.1	0.1	0.1
k_{delay}	0.666 ± 0.112	0.553 ± 0.083	0.695 ± 0.096
SF_{38}	0.937 ± 0.066	0.885 ± 0.063	0.979 ± 0.092
SF_{40}	0.933 ± 0.043	0.916 ± 0.078	0.977 ± 0.130
SF_{42}	0.972 ± 0.102	0.879 ± 0.021	0.912 ± 0.151

irreversible loss of each soluble Aβ isoform that was not recovered in CSF. The rate constants for transfer between compartments in the model were optimized for each participant, and mean values for each parameter are summarized in Table 1. The model describes three fundamental processes that affect Aβ kinetics—production, reversible exchange, and irreversible loss—and accounts for the effect of these processes on CSF Aβ concentrations.

Increased Aβ42 and Aβ42/Aβ40 production with PSEN mutations regardless of amyloid deposition

The mutation carriers had an 18% higher absolute Aβ42 production rate ($P < 0.05$, for mutation effect) and a 24% higher Aβ42/Aβ40 production rate ratio ($P < 0.0001$, for mutation effect) than the nonmutation carriers, whereas amyloid load as measured by PIB-PET did not have a significant effect on Aβ42 production rate (Table 2, Fig. 3A, and fig. S5). There were no differences in Aβ38 or Aβ40 absolute production rates or the Aβ38/Aβ40 production rate ratio between carrier and noncarrier groups (Table 2).

Exchange process required to fit Aβ kinetic curves

To optimally fit the shape and peak magnitude of Aβ isoform enrichment time courses, a compartment was required to model reversible exchange of newly synthesized labeled Aβ peptides with a preexisting pool of unlabeled Aβ (Fig. 2). The exchange process was of minimal magnitude in nonmutation carriers, in which only ~10% of the flux of newly synthesized Aβ38, Aβ40, or Aβ42 underwent exchange (Table 2). The percent of Aβ38 and Aβ40 that underwent exchange was not significantly different between mutation carriers and noncarriers. However, the exchange for Aβ42 was significantly greater in carriers compared to the noncarriers (51 ± 58% versus 6 ± 12% of flux, respectively; $P = 0.004$, for mutation effect; $P = 0.001$, for PIB status) (Table 2). The exchange process for Aβ42, combined with a faster turnover rate of Aβ42 (see below), provided an excellent fit to the entire shape of the Aβ42 enrichment time course in all groups including mutation carriers with amyloid deposition (mean R^2 for all participants of 0.994, 0.995, and 0.987 for Aβ38, Aβ40, and Aβ42, respectively).

Higher irreversible loss of Aβ42 in amyloid deposition

The FTR (pools per hour) of soluble Aβ is the rate constant for irreversible loss of soluble Aβ to all metabolic fates; this process is kinetically distinct from reversible exchange. The physiology of the system suggests that the FTR includes irreversible losses to the CSF or bloodstream, degradation, and deposition into amyloid plaques. The Aβ40 FTR was significantly slower in PIB$^+$ compared to PIB$^-$ participants ($P = 0.024$, for PIB MCBP score) and trended toward significance for Aβ38 ($P = 0.054$, for PIB MCBP score), but neither was affected by mutation status (Table 2 and Fig. 3B). This decreased turnover rate correlated with the extent of amyloidosis measured by PET PIB. In contrast, Aβ42 FTR trended toward an increase in mutation carriers ($P = 0.065$, for mutation effect) independent of amyloid load (Table 2 and Fig. 3B). The Aβ38/Aβ40 FTR ratio was not significantly different between noncarrier and mutation carrier groups, but the Aβ42/Aβ40 FTR ratio was 65% higher in mutation carriers ($P < 0.002$, for both mutation status and PIB MCBP score) (Table 2 and Fig. 3B).

Decreased CSF Aβ42 concentrations only during amyloid deposition

The measured basal concentrations of CSF Aβ isoforms were compared by mutation status and PIB MCBP score (Table 2 and Fig. 3C). The Aβ42 CSF concentration and the Aβ42/Aβ40 CSF concentration ratio were significantly reduced in association with amyloid deposition ($P = 0.003$, for PIB MCBP score; not significant by mutation status), whereas there were no differences between groups for the CSF Aβ38, Aβ40, or Aβ38/Aβ40 concentration ratio (Table 2).

DISCUSSION

Our study of in vivo CNS Aβ isoform kinetics in participants with *PSEN* mutations confirms the hypothesis that the production rate of Aβ42 is increased relative to Aβ40 in humans with *PSEN* mutations associated with ADAD, and also revealed increased exchange of soluble Aβ42 and increased irreversible loss of soluble Aβ42 associated with the presence of fibrillar amyloid plaques. The finding of increased Aβ42 production was predicted by some in vitro studies (*11*, *12*) and evidence of altered γ-secretase function in carriers of *PSEN1* or *PSEN2* ADAD mutations (*24*). Here, we directly quantify increased Aβ42 production in vivo in humans because of mutations that cause ADAD, and confirm that such mutations increase CNS Aβ42 production rates in vivo. The ratio of Aβ42 to Aβ40 production rates was greater than 15% for almost all mutation carriers (average, 17.4%), whereas noncarriers were less than 15% (average, 14%), suggesting tight physiological control that is disrupted in the presence of a mutation. There was a ~25% relative increase in Aβ42 to Aβ40 production rate in mutation carriers, which correlates

Table 2. CSF Aβ isoform concentrations and selected model kinetic parameters. Parameters were determined on the basis of the best fit to a compartmental model of Aβ turnover and production. Outcomes were compared by mutation status using ANOVA after adjusting for fibrillar amyloid deposition by treating PIB MCBP score as a covariate. Kinetic parameters are identified with terminology (Fig. 2). $P < 0.05$, in bold. IP, immunoprecipitation.

	Noncarriers (n = 12)	Mutation carriers (n = 11)	P*	
Production rate, ng/hour (for example, C99 pool size × $k_{Aβ42}$)			Mutation status	PIB MCBP score
Aβ38	106 (41)	111 (50)	0.603	0.571
Aβ40	418 ± 83	452 ± 138	0.621	0.901
Aβ42	57 (19)	67 (35)	**0.038**	0.769
Aβ38/Aβ40 ratio	0.267 (0.021)	0.252 (0.052)	0.692	0.179
Aβ42/Aβ40 ratio	0.140 ± 0.011	0.174 ± 0.020	**9×10^{-5}**	0.312
Percentage of flux going to exchange (%)†			Mutation status	PIB status
Aβ38	9.8 ± 16.6	0‡	0.190	0.376
Aβ40	7.8 ± 13.9	1.2 ± 4.1	0.316	0.249
Aβ42	5.8 ± 11.5	50.8 ± 57.6	**0.004**	**0.001**
Permanent loss of soluble Aβ to all fates (FTR) (pools per hour) (for example, $v_{42} + k_{CSF}$)			Mutation status	PIB MCBP score
Aβ38	0.144 ± 0.046	0.124 ± 0.049	0.802	0.054
Aβ40	0.156 (0.055)	0.109 (0.035)	0.990	**0.024**
Aβ42	0.147 (0.049)	0.198 (0.086)	0.065	0.548
Aβ38/Aβ40 ratio	0.964 ± 0.038	1.013 ± 0.047	0.157	0.115
Aβ42/Aβ40 ratio	0.942 ± 0.080	1.553 ± 0.382	**0.0016**	**0.0003**
CSF concentration by IP-MS (ng/ml)			Mutation status	PIB MCBP score
Aβ38	2.05 (0.69)	1.82 (1.00)	0.296	0.105
Aβ40	7.15 ± 1.80	7.79 ± 1.89	0.199	0.272
Aβ42	1.01 (0.39)	0.80 (0.52)	0.537	**0.007**
Aβ38/Aβ40 ratio	0.272 ± 0.014	0.256 ± 0.053	0.803	0.068
Aβ42/Aβ40 ratio	0.149 ± 0.013	0.121 ± 0.042	0.720	**0.003**

*P values by ANOVA based on mutation status with PIB MCBP score as a covariate. †Analyzed by nonparametric Mann-Whitney U test because of nonnormal distribution, based on mutation status and PIB status (rather than PIB MCBP score). ‡No exchange observed in any subject.

with the 40% decrease in Aβ production because of a mutation that is protective for the development of AD (*7*). Changes in the Aβ42 to Aβ40 production rate ratio are likely to have a large impact on the rate of Aβ42 deposition into plaques because in vitro studies have demonstrated that even relatively small changes in the Aβ42/Aβ40 ratio significantly affect aggregation kinetics and morphology (*15*) that could promote plaque formation. The Aβ42/Aβ40 ratio and the total amount of Aβ42 have been hypothesized to affect the age of onset of ADAD (*25*). Some *PSEN* mutations in cultured cells in vitro have been reported to decrease Aβ40 production or loss of overall Aβ production (*16*); however, our in vivo SILK studies did not confirm decreased Aβ40 or total Aβ production.

Our finding of a faster irreversible FTR of soluble Aβ42 relative to Aβ38 or Aβ40 in the presence of *PSEN* mutations or plaques was not anticipated. This faster relative FTR was a primary factor causing the Aβ42 isotopic enrichment curve to peak earlier than Aβ38 or Aβ40 in the presence of amyloidosis (Fig. 1). We cannot determine the physiological mechanisms that underlie this irreversible FTR, but it includes all losses of soluble Aβ peptides including transport into CSF or plasma, proteolytic degradation, and deposition into amyloid plaques. The rate constant for transport to CSF is likely to be similar for all Aβ isoforms because the transport of soluble Aβ isoforms to CSF is driven by fluid flow (*26*). Therefore, the faster relative FTR of Aβ42 in the presence of plaques implies a greater loss of Aβ42 from the system to fates other than CSF. Although we cannot identify the specific fates of peptides permanently lost from the system, our observations are consistent with increased deposition of Aβ42 into amyloid plaques (*27*, *28*) relative to Aβ38 and Aβ40, which subsequently causes increased Aβ42 in brain plaques (*29*), as shown in video S1, and a reduction in the amount of Aβ42 recovered in CSF (*30*). Our finding of increased irreversible FTR of Aβ42 in subjects with *PSEN* mutations but no amyloid load suggests that increased Aβ42 deposition may be occurring in these subjects, and SILK studies of Aβ42 turnover kinetics may provide a sensitive window into altered processes before amyloidosis is detectable by PET PIB.

Another unanticipated finding was a reversible exchange process whereby a portion of newly synthesized (that is, isotopically labeled) peptides exchange with preexisting unlabeled Aβ. The structures of the preexisting unlabeled Aβ cannot be determined from this tracer study, but they could potentially consist of oligomers or aggregates (*31*, *32*) or may reflect reversible binding of Aβ42 to the surface of

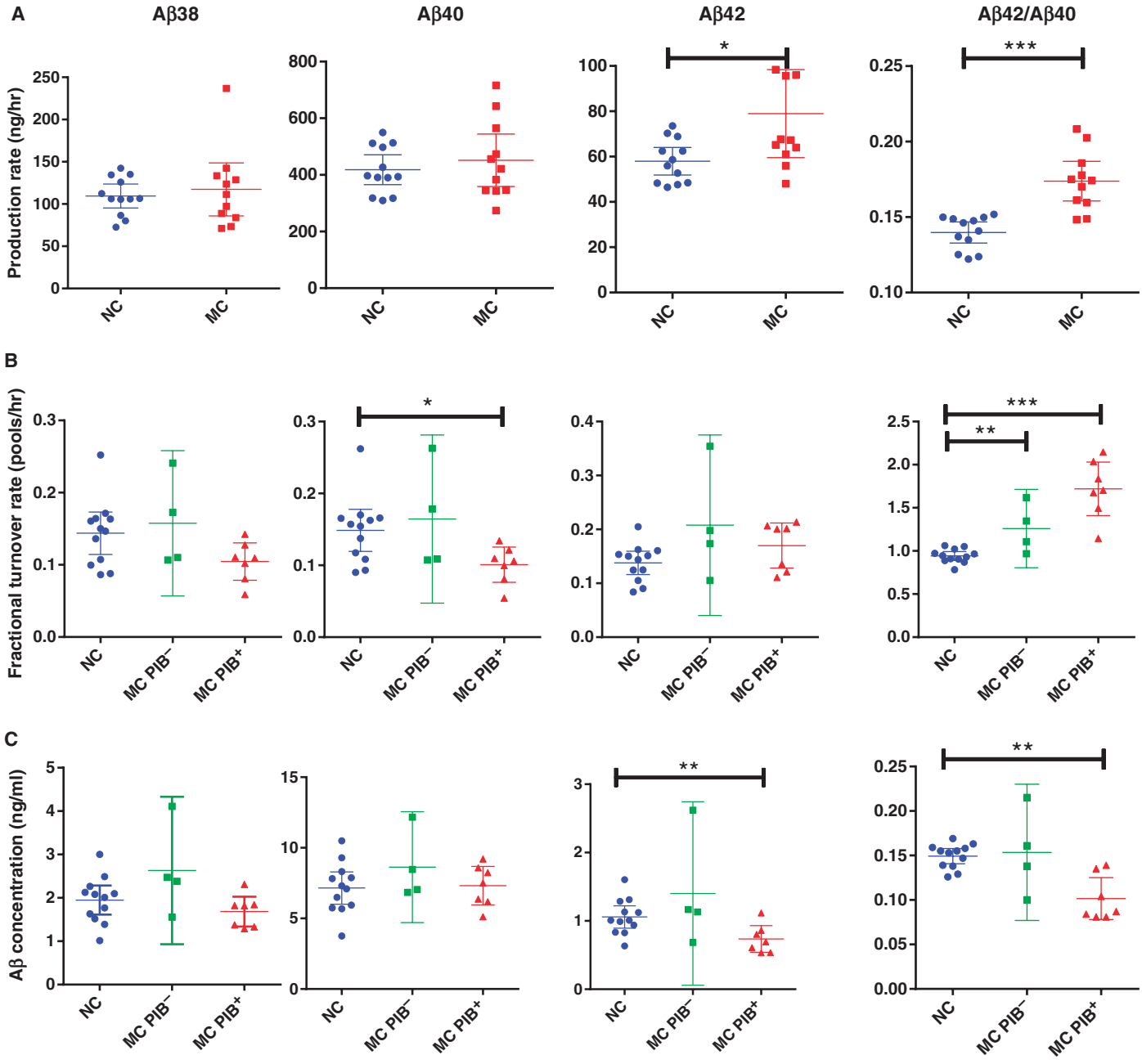

Fig. 3. Aβ concentrations and selected kinetic parameters. (**A** to **C**) Parameters for Aβ production rate (A), FTR (B), and baseline CSF concentrations (C) are shown for each group by mutation status and without (PIB^-) or with (PIB^+) evidence of amyloid deposition. Each parameter was measured for Aβ38 (first column), Aβ40 (second column), Aβ42 (third column), and the Aβ42/Aβ40 ratio (fourth column), and compared by mutation status and amyloid deposition. Error bars indicate 95% confidence intervals. Mutation status compared when amyloid deposition did not affect magnitude or significance. *$P < 0.05$, **$P < 0.01$, ***$P < 0.001$, ANOVA based on mutation status with PIB MCBP score as a covariate. Blue circles, noncarriers; green squares, mutation carrier PIB^- ($MC\ PIB^-$); red triangles, mutation carrier PIB^+ ($MC\ PIB^+$). Each point represents one participant.

amyloid plaques before structural alterations cause permanent assimilation into plaques (*33*, *34*).

We previously reported that late-onset AD was associated with a slower clearance rate for Aβ40 and Aβ42 based on a monoexponential slope applied to the terminal phase (24 to 36 hours) of the SILK enrichment time course (*18*). The present study used a compartmental model to fit the SILK enrichment time courses over the full experimental period (0 to 36 hours) in a manner consistent with known physiological processes (*35*). This compartmental model confirms the previous report that the FTR is slower for Aβ40 with increased insoluble amyloid plaque deposition (Table 2). The exchange process described by our compartmental model was minimal for Aβ38 and Aβ40 in the presence

or absence of amyloid plaques (Table 2), and thus, the terminal tail approximates a monoexponential shape for these isoforms. The observation that the irreversible FTRs of Aβ38 and Aβ40 are negatively correlated with PIB MCBP score (Table 2) suggests that the presence of plaques substantially alters physiological processes (for example, fluid flow perfusion through brain tissue) and thus retards the transfer of soluble Aβ peptide from the brain to CSF. An outcome of this decreased transport to the CSF may be loss of the normal physiological diurnal pattern of CSF Aβ concentrations (*36*, *37*).

Several caveats about the compartmental model limit the ability to completely resolve the system. Flow processes likely dictate the rate at which Aβ peptides transit from brain to the lumbar space. These processes are approximated here as a sequential series of compartments. More elaborate models that account for brain and subarachnoid space anatomy and flow may allow more accurate determination of the rates of Aβ peptide irreversible loss and production. The current data set is also not rich enough to identify the rates of production and irreversible loss of APP and C99. Additional kinetic data relevant to the production and irreversible loss of APP and C99 would improve the estimation of Aβ production and irreversible loss rate constants. Also, measurement of concentrations of various Aβ peptides has a large impact on the estimates of the production rate constants for the Aβ peptides.

The present study also confirms that the terminal slope of the Aβ42 enrichment curve is slower in the presence of plaques. We observed that Aβ42 irreversible FTR was increased in the presence of *PSEN* mutations independent of plaque load. The SILK tracer technique thus reveals abnormalities in Aβ42 before plaques are detectable by PET PIB. Indeed, three of the four mutation carriers who did not have detectable amyloid plaques by PET PIB had features of Aβ42 kinetics that were more similar to mutation carriers with amyloid plaques than to noncarriers, including Aβ42/Aβ40 FTR ratio >1.1, and evidence of Aβ42 exchange (fig. S2). These features strongly suggest that plaque development or some form of Aβ aggregation has been initiated in these individuals, but fibrillar plaque load has not reached the threshold of PET PIB detection. In contrast, only one mutation carrier who was PET PIB–negative had no evidence of Aβ42 exchange. This participant also had the highest Aβ42/Aβ40 CSF concentration ratio (0.215; fig. S4) of all participants in our study (compare to figs. S2 and S3; this ratio was 27% higher than the next highest concentration ratio observed in individual participants, 0.169), demonstrating that elevated Aβ42/Aβ40 CSF concentration ratios are only observed in ADAD persons in the absence of amyloid plaques. Because amyloid deposition in the caudate may be one of the earliest deposition events, we evaluated caudate PIB as a sensitive measure of amyloid deposition. The caudate PIB and MCBP PIB were highly correlated with each other with a Pearson correlation coefficient of 0.94 ($P = 5 \times 10^{-11}$); no kinetic parameters changed significance with amyloidosis as measured by caudate PIB.

Our findings offer a context for the recent report that CSF Aβ42 concentration is elevated in ADAD individuals decades before predicted age for onset of clinical symptoms of dementia, and then drops below normal as plaques develop (*2*, *38*) (see Fig. 4 for schematic of proposed process). Our finding of increased Aβ42 production in mutation carriers regardless of the amount of amyloid deposition indicates that increased Aβ42 production precedes amyloid deposition, and likely occurs decades before the onset of dementia and is possibly present throughout life. The long delay in the emergence of plaque deposits

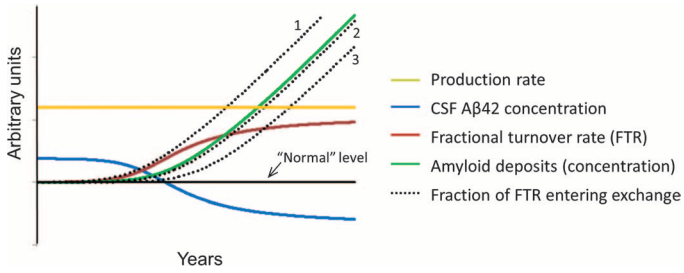

Fig. 4. Potential scheme for the time course of plaque deposition in ADAD. The solid black line signifies normal for each measure. The production rate of Aβ42 relative to Aβ40 (gold) remains constant throughout life before and during plaque deposition (production rate was different by mutation status but not by amyloid deposition). CSF concentration of Aβ42 (blue) starts elevated above normal because of overproduction and then decreases to below normal because of an increase in the FTR (red) of Aβ42 relative to Aβ40. As the amount of amyloid plaques increases over time (green), the extent of Aβ42 exchange (dotted) may precede (for example, if due to oligomer formation), follow closely, or lag behind amyloid deposition (for example, if due to reversible interaction with amyloid plaques).

of Aβ42 even in the presence of overproduction of Aβ42 suggests the presence of an initial slow process (for example, initial Aβ nucleation event in which monomeric Aβ forms small aggregates) followed by a growth phase of Aβ polymerization (*39*). We therefore hypothesize that Aβ42 production rate (solid gold line, Fig. 4) remains above "normal" (solid black line) throughout life because of their *PSEN* genotype. ADAD individuals have an increased irreversible loss of soluble Aβ42 (FTR solid red line, Fig. 4) that tracks or precedes PET-detectable amyloid deposition, consistent with a faster removal of soluble Aβ42 as it is deposited into plaques. This results in a decreased recovery of Aβ42 in the CSF, accounting for the decrease in CSF Aβ42 concentration (solid blue line, Fig. 4) as plaque development proceeds (solid green line, Fig. 4). The physiological identity of the pool(s) in exchange with newly labeled soluble Aβ42 identified by SILK (dotted black lines, Fig. 4) cannot be determined in this study. If exchange occurs with micelles or oligomers, exchange may precede PET-detectable amyloid deposition (dotted line 1, Fig. 4). If exchange is with plaque surfaces, it may track or even lag behind amyloid deposition (dotted lines 2 and 3, Fig. 4). Future studies with greater numbers of participants or longitudinal designs will be required to resolve this question.

Although ADAD represents less than 1% of all AD cases, it has been informative for elucidating the pathophysiology of AD and can manifest as late-onset AD indistinguishable from the more idiopathic forms (*40*). The findings of this study further support the amyloid hypothesis and provide quantitative estimates of lifelong increases in Aβ42 production that may cause AD in humans. Further, these results indicate profound changes in Aβ kinetics in the presence of amyloid plaques. With increased understanding of the pathogenic causes of AD and the quantitative changes associated with AD pathology, it is hoped that better tests and directed therapeutics can be developed in the future.

MATERIALS AND METHODS

Study design

This study took place at the Washington University School of Medicine in St. Louis and was approved by the Human Research Protection Office.

All participants completed informed written consent. Two groups of volunteers were enrolled in the study: (i) ADAD mutation carriers either with ($n = 7$) or without ($n = 4$) amyloid deposition and (ii) related family members at risk for carrying a mutation but who do not carry ADAD mutations ($n = 12$).

Binding of [^{11}C]PIB-PET was used to test for deposition of amyloid plaques in the brain (*23*). Binding potentials using the cerebellum as a reference region were determined for the prefrontal cortex, precuneus, lateral temporal cortex, and gyrus rectus. The PIB MCBP score was determined by averaging these binding potentials together. A PIB MCBP score of 0.18 was considered evidence of amyloid deposition (PIB$^+$), and a PIB MCBP score of less than 0.18 was considered to be amyloid deposition–negative (PIB$^-$). The highest PIB MCBP score in noncarriers was 0.12.

Participant demographics

Twenty-three participants from nine pedigrees (*PSEN1* Ala79Val, Leu226Arg, His163Arg, Met146Leu, Met139Ile, Gly217Arg, Ala246Glu, and *PSEN2* Asn141Ile) completed Aβ SILK studies. Twelve (52%) of the participants were male. The average age of mutation carriers was 43.2 ± 12.7, and that of noncarriers was 47.7 ± 14.8 ($P > 0.05$). Eight *PSEN1* mutation carriers and three *PSEN2* mutation carriers were included in the analysis with sibling controls. Two mutation carriers were rated as having prodromal dementia and one with mild dementia. Eight mutation carriers were cognitively asymptomatic, as were all noncarriers. Seven mutation carriers were PIB$^+$, and four of the mutation carriers and all noncarriers were PIB$^-$; the average PIB MCBP score was significantly different between groups, 0.03 ± 0.04 versus 0.43 ± 0.45 for noncarriers and mutation carriers, respectively ($P = 0.005$). At least one APOE ε4 allele was present in 33% ($n = 4$) of the noncarrier group, 25% of the mutation carrier PIB$^-$ group, and 28% of the mutation carrier PIB$^+$ group ($P > 0.05$).

Sample collection

The SILK clinical study followed the procedure previously described (*41*). Briefly, intravenous and intrathecal lumbar catheters were placed between 7:30 and 9:00 a.m., and the collection of samples was started between 8:00 and 9:30 a.m. After initial CSF and plasma baseline samples were collected, participants were infused with a bolus of L-[U-$^{13}C_6$]leucine (3 mg/kg) for 10 min, followed by 2 mg/kg per hour for the remainder of the first 9 hours. For the 36 hours of the study, 6 ml of CSF was obtained every hour; afterward, the catheters were removed, and participants remained on bed rest for 12 hours. Aliquots of CSF were frozen at −80°C immediately in 1-ml polypropylene tubes after being collected. Venous blood samples (12 ml) were obtained at hourly intervals from 1 to 13 hours and then at 17 and 36 hours, and plasma was stored at −80°C for the determination of plasma leucine enrichment.

Analysis of CSF samples

All procedures relating to clinical studies, sample processing, and sample analysis were performed blinded to mutation, clinical, and amyloid status. At each hour of collection, 1 ml of CSF was thawed, and Aβ was immunopurified and isotopic enrichment of Aβ isoforms was measured with liquid chromatography–mass spectrometry (MS) similar to previous studies (*18*), except for dedicated measurement of Aβ38, Aβ40, and Aβ42 C-terminal peptides.

Measurements of Aβ38, Aβ40, and Aβ42 C-terminal peptides

A mid-domain antibody (HJ5.1, anti–A$\beta_{13–28}$) was covalently bound to CNBr Sepharose beads and stored in a 50% slurry of 0.02% phosphate-buffered saline/azide at 4°C. The immunopurification mixture was composed of 800 μl of CSF; 20 μl of a solution containing $^{12}C^{15}N$ Aβ40, Aβ42, and Aβ38 for quantification by internal standard; and 12.5 μl of 100× protease inhibitor, 110 μl of 5 M guanidine, and 30 μl of antibody-bead slurry. Beads were rotated in an Eppendorf Axygen tube for 2 hours at room temperature and rinsed with 0.5 M guanidine followed by two rinses of 25 mM ammonium bicarbonate. All liquid was removed by aspiration, and then neat formic acid was added to elute Aβ from the antibody-bead complex. The formic acid supernatant was transferred to a new polypropylene tube and dried in a vacuum dryer (Labconco CentriVap). The sample was reconstituted with 25 μl of 25 mM ammonium bicarbonate and digested with 2.5 ng of Lys-N overnight at 37°C. This solution was dried in the speed vacuum and resuspended in 10% formic acid and 20% dimethyl sulfoxide. Three microliters of this sample was injected into a nanoACQUITY Ultra Performance Liquid Chromatography system and then analyzed by a XEVO TQ-S mass spectrometer (Waters). MassLynx V4.1 was used to quantify the MS data. For determination of plasma $^{13}C_6$-leucine enrichment, amino acids were recovered from plasma with cation exchange chromatography and converted to *N*-heptafluorobutyryl *n*-propyl ester derivatives, and isotopic enrichment [mass/charge ratio (*m/z*) 349 and 355] was measured with gas chromatography (GC)–negative chemical ionization–MS (Agilent 6890N Gas Chromatograph and Agilent 5973N Mass Selective Detector) as described (*42*). The GC-MS instrument response was calibrated with gravimetric standards of known isotope enrichment.

Compartmental model for Aβ38, Aβ40, and Aβ42 kinetics

A comprehensive steady-state compartmental model that accounts for the full time course of Aβ38, Aβ40, and Aβ42 enrichments and CSF concentrations was developed; a diagram of the model is shown in Fig. 2. The model consists of a series of interconnected compartments with first-order rate constants that describe the transfer of labeled species between compartments. Modeling was performed with SAAM II (Resource for Kinetic Analysis, University of Washington, Seattle, WA). The model consists of three parallel arms, one for each Aβ isoform. The enrichments of plasma leucine and CSF Aβ peptides were measured at frequent time intervals (indicated by solid triangles). Plasma leucine is used as the tracer precursor for CSF Aβ peptides because we have shown that, given a sufficiently long infusion, CSF Aβ enrichments essentially match that of plasma leucine in monkeys (*43*). A "forcing function" was used to describe the time course of plasma $^{13}C_6$-leucine enrichment with a linear interpolation between measured samples.

Preliminary modeling revealed that the isotopic enrichment time course for each Aβ isoform could be optimally described by a single compartment coupled with a long time delay that consisted of five subcompartments. On the basis of known physiology, two of these delay compartments (representing APP and C99 peptides) were placed in front of the compartments that represent the brain "soluble" Aβ peptides because in vivo tracer studies in mice show that APP and C99 have relatively long half-lives (~3 hours) (*44*) that should contribute to the overall time delay before labeled Aβ is detected at the lumbar sampling site. The remaining three delay compartments were placed after the soluble Aβ compartments to represent perfusion of labeled peptides through brain tissue and heterogeneous CSF fluid transport processes.

Given that preliminary modeling indicated that a single time delay process could be identified within the data, the turnover rates for APP, C99, and each of the three CSF delay compartments were set to a single adjustable parameter that affects the overall time delay.

The model takes into consideration that some of the C99 and soluble Aβ peptides are metabolized to fates other than Aβ peptides that appear at the CSF sampling site. The physiological nature of these other losses for soluble Aβ peptides is unknown but includes all processes that remove soluble peptides irreversibly, for example, deposition into plaques, cellular uptake, and proteolytic degradation. A compartment in exchange with the soluble Aβ peptide was necessary to optimally fit the sigmoid shape of the CSF Aβ enrichment time courses after the peak enrichment, particularly for Aβ42 in the mutation carrier PIB^+ group; this exchange process was added for an isoform only if it improved the Akaike information criteria (AIC) of the fit as provided by SAAM II. A scaling factor was applied to each of the Aβ isoform enrichments if it improved the AIC to account for small amounts of isotopic dilution between plasma leucine and the biosynthetic precursor pool (generally <5%) or to correct for minor calibration errors (generally <10%) in the measurement of isotope enrichments of plasma leucine or Aβ peptides.

On the basis of the optimized kinetic parameters that describe the shape and magnitude of the CSF Aβ enrichment time course, the model determines the rate constant (pools per hour) for production of each Aβ peptide from their common C99 precursor to accurately project the measured baseline CSF Aβ peptide concentrations. The model projects the steady-state masses (ng) within and the flux rates (ng/hour) between all compartments for each Aβ isoform.

Statistical analyses

Ratios of isotopic enrichments between peptides at all time points were analyzed by repeated-measures ANOVA. When the time by group interaction was significant, enrichment ratios at individual time points were analyzed by ANOVA with a linear contrast to test for significant group effects. ANOVA was performed with a mutation status main affect, adjusting for PIB MCBP score as a covariate. Variables were tested for normal distribution by Shapiro-Wilk criterion; variables that were not normally distributed were log-transformed before performing ANOVA. The distribution of rate constants describing the exchange process revealed by the model was analyzed by Mann-Whitney *U* test because log transformation did not normalize the distribution. Statistics were performed with IBM SPSS version 20. A P value of <0.05 was considered to be statistically significant. Unless otherwise noted, results shown are mean ± SD for normally distributed variables or as median with interquartile range for nonnormally distributed variables. Graph generations were performed in GraphPad Prism version 5.01 for Windows (GraphPad Software).

Movie methods

A video illustrating the isotope labeling model for soluble Aβ42 and Aβ40 was created with Matplotlib (*41*). Compartments for soluble, exchange, and irreversible loss (plaque) are shown over the MNI152 template image included as part of the FMRIB Software Library (*42*). The location of the fibrillar plaque compartment in the illustration was determined by thresholding the average PIB image for PIB^+ mutation carriers. The growth of the soluble, exchange, and irreversible loss compartments followed the normalized production rates for each peptide. Note that the sizes of the Aβ compartments are greatly exaggerated for visualization purposes.

SUPPLEMENTARY MATERIALS

www.sciencetranslationalmedicine.org/cgi/content/full/5/189/189ra77/DC1

Fig. S1. Time course of plasma leucine isotopic enrichment.

Fig. S2. Isotopic enrichment time courses of CSF Aβ peptides in individual nonmutation carrier participants.

Fig. S3. Isotopic enrichment time courses of CSF Aβ peptides in mutation carrier participants with amyloid plaques (PIB^+).

Fig. S4. Isotopic enrichment time courses of CSF Aβ peptides in mutation carrier participants without amyloid plaques (PIB^-).

Fig. S5. Whisker box plot and scatter plot of concentrations and selected kinetic parameters.

Video S1. Animated illustration of isotope labeling time course and amyloid deposition.

REFERENCES AND NOTES

1. R. J. Bateman, P. S. Aisen, B. De Strooper, N. C. Fox, C. A. Lemere, J. M. Ringman, S. Salloway, R. A. Sperling, M. Windisch, C. Xiong, Autosomal-dominant Alzheimer's disease: A review and proposal for the prevention of Alzheimer's disease. *Alzheimers Res. Ther.* **3**, 1 (2011).
2. R. J. Bateman, C. Xiong, T. L. S. Benzinger, A. M. Fagan, A. Goate, N. C. Fox, D. S. Marcus, N. J. Cairns, X. Xie, T. M. Blazey, D. M. Holtzman, A. Santacruz, V. Buckles, A. Oliver, K. Moulder, P. S. Aisen, B. Ghetti, W. E. Klunk, E. McDade, R. N. Martins, C. L. Masters, R. Mayeux, J. M. Ringman, M. N. Rossor, P. R. Schofield, R. A. Sperling, S. Salloway, J. C. Morris, Clinical and biomarker changes in dominantly inherited Alzheimer's disease. *N. Engl. J. Med.* **367**, 795–804 (2012).
3. J. Hardy, D. J. Selkoe, The amyloid hypothesis of Alzheimer's disease: Progress and problems on the road to therapeutics. *Science* **297**, 353–356 (2002).
4. C. Haass, B. De Strooper, The presenilins in Alzheimer's disease—Proteolysis holds the key. *Science* **286**, 916–919 (1999).
5. R. Wang, D. Sweeney, S. E. Gandy, S. S. Sisodia, The profile of soluble amyloid β protein in cultured cell media. Detection and quantification of amyloid β protein and variants by immunoprecipitation-mass spectrometry. *J. Biol. Chem.* **271**, 31894–31902 (1996).
6. D. L. Miller, I. A. Papayannopoulos, J. Styles, S. A. Bobin, Y. Y. Lin, K. Biemann, K. Iqbal, Peptide compositions of the cerebrovascular and senile plaque core amyloid deposits of Alzheimer's disease. *Arch. Biochem. Biophys.* **301**, 41–52 (1993).
7. T. Jonsson, J. K. Atwal, S. Steinberg, J. Snaedal, P. V. Jonsson, S. Bjornsson, H. Stefansson, P. Sulem, D. Gudbjartsson, J. Maloney, K. Hoyte, A. Gustafson, Y. Liu, Y. Lu, T. Bhangale, R. R. Graham, J. Huttenlocher, G. Bjornsdottir, O. A. Andreassen, E. G. Jönsson, A. Palotie, T. W. Behrens, O. T. Magnusson, A. Kong, U. Thorsteinsdottir, R. J. Watts, K. Stefansson, A mutation in APP protects against Alzheimer's disease and age-related cognitive decline. *Nature* **488**, 96–99 (2012).
8. A. Rovelet-Lecrux, D. Hannequin, G. Raux, N. L. Meur, A. Laquerrière, A. Vital, C. Dumanchin, S. Feuillette, A. Brice, M. Vercelletto, F. Dubas, T. Frebourg, D. Campion, APP locus duplication causes autosomal dominant early-onset Alzheimer disease with cerebral amyloid angiopathy. *Nat. Genet.* **38**, 24–26 (2006).
9. A. Goate, M.-C. Chartier-Harlin, M. Mullan, J. Brown, F. Crawford, L. Fidani, L. Giuffra, A. Haynes, N. Irving, L. James, R. Mant, P. Newton, K. Rooke, P. Roques, C. Talbot, M. Pericak-Vance, A. Roses, R. Williamson, M. Rossor, M. Owen, J. Hardy, Segregation of a missense mutation in the amyloid precursor protein gene with familial Alzheimer's disease. *Nature* **349**, 704–706 (1991).
10. E. Levy-Lahad, E. M. Wijsman, E. Nemens, L. Anderson, K. A. Goddard, J. L. Weber, T. D. Bird, G. D. Schellenberg, A familial Alzheimer's disease locus on chromosome 1. *Science* **269**, 970–973 (1995).
11. D. Scheuner, C. Eckman, M. Jensen, X. Song, M. Citron, N. Suzuki, T. D. Bird, J. Hardy, M. Hutton, W. Kukull, E. Larson, E. Levy-Lahad, M. Viitanen, E. Peskind, P. Poorkaj, G. Schellenberg, R. Tanzi, W. Wasco, L. Lannfelt, D. Selkoe, S. Younkin, Secreted amyloid β-protein similar to that in the senile plaques of Alzheimer's disease is increased in vivo by the presenilin 1 and 2 and *APP* mutations linked to familial Alzheimer's disease. *Nat. Med.* **2**, 864–870 (1996).
12. D. R. Borchelt, G. Thinakaran, C. B. Eckman, M. K. Lee, F. Davenport, T. Ratovitsky, C.-M. Prada, G. Kim, S. Seekins, D. Yager, H. H. Slunt, R. Wang, M. Seeger, A. I. Levey, S. E. Gandy, N. G. Copeland, N. A. Jenkins, D. L. Price, S. G. Younkin, S. S. Sisodia, Familial Alzheimer's disease–linked presenilin 1 variants elevate Aβ1–42/1–40 ratio in vitro and in vivo. *Neuron* **17**, 1005–1013 (1996).
13. J. M. Ringman, S. G. Younkin, D. Pratico, W. Seltzer, G. M. Cole, D. H. Geschwind, Y. Rodriguez-Agudelo, B. Schaffer, J. Fein, S. Sokolow, E. R. Rosario, K. H. Gylys, A. Varpetian, L. D. Medina, J. L. Cummings, Biochemical markers in persons with preclinical familial Alzheimer disease. *Neurology* **71**, 85–92 (2008).
14. J. S. Kauwe, S. Jacquart, S. Chakraverty, J. Wang, K. Mayo, A. M. Fagan, D. M. Holtzman, J. C. Morris, A. M. Goate, Extreme cerebrospinal fluid amyloid β levels identify family with late-onset Alzheimer's disease presenilin 1 mutation. *Ann. Neurol.* **61**, 446–453 (2007).
15. I. Kuperstein, K. Broersen, I. Benilova, J. Rozenski, W. Jonckheere, M. Debulpaep, A. Vandersteen, I. Segers-Nolten, K. Van Der Werf, V. Subramaniam, D. Braeken, G. Callewaert, C. Bartic, R. D'Hooge, I. C. Martins, F. Rousseau, J. Schymkowitz, B. De Strooper, Neurotoxicity of Alzheimer's disease Aβ peptides is induced by small changes in the $Aβ_{42}$ to $Aβ_{40}$ ratio. *EMBO J.* **29**, 3408–3420 (2010).
16. J. Shioi, A. Georgakopoulos, P. Mehta, Z. Kouchi, C. M. Litterst, L. Baki, N. K. Robakis, FAD mutants unable to increase neurotoxic Aβ 42 suggest that mutation effects on neurodegeneration may be independent of effects on Aβ. *J. Neurochem.* **101**, 674–681 (2007).

17. M. Moonis, J. M. Swearer, M. P. Dayaw, P. St George-Hyslop, E. Rogaeva, T. Kawarai, D. A. Pollen, Familial Alzheimer disease: Decreases in CSF $A\beta_{42}$ levels precede cognitive decline. *Neurology* **65**, 323–325 (2005).
18. K. G. Mawuenyega, W. Sigurdson, V. Ovod, L. Munsell, T. Kasten, J. C. Morris, K. E. Yarasheski, R. J. Bateman, Decreased clearance of CNS β-amyloid in Alzheimer's disease. *Science* **330**, 1774 (2010).
19. N. Andreasen, C. Hesse, P. Davidsson, L. Minthon, A. Wallin, B. Winblad, H. Vanderstichele, E. Vanmechelen, K. Blennow, Cerebrospinal fluid β-amyloid(1-42) in Alzheimer disease: Differences between early- and late-onset Alzheimer disease and stability during the course of disease. *Arch. Neurol.* **56**, 673–680 (1999).
20. A. M. Fagan, M. A. Mintun, R. H. Mach, S. Y. Lee, C. S. Dence, A. R. Shah, G. N. LaRossa, M. L. Spinner, W. E. Klunk, C. A. Mathis, S. T. DeKosky, J. C. Morris, D. M. Holtzman, Inverse relation between in vivo amyloid imaging load and cerebrospinal fluid $A\beta_{42}$ in humans. *Ann. Neurol.* **59**, 512–519 (2006).
21. G. Nikisch, A. Hertel, B. Kiessling, T. Wagner, D. Krasz, E. Hofmann, G. Wiedemann, Three-year follow-up of a patient with early-onset Alzheimer's disease with presenilin-2 N141I mutation—Case report and review of the literature. *Eur. J. Med. Res.* **13**, 579–584 (2008).
22. B. De Strooper, Loss-of-function presenilin mutations in Alzheimer disease. Talking Point on the role of presenilin mutations in Alzheimer disease. *EMBO Rep.* **8**, 141–146 (2007).
23. M. A. Mintun, G. N. Larossa, Y. I. Sheline, C. S. Dence, S. Y. Lee, R. H. Mach, W. E. Klunk, C. A. Mathis, S. T. DeKosky, J. C. Morris, [^{11}C]PIB in a nondemented population: Potential antecedent marker of Alzheimer disease. *Neurology* **67**, 446–452 (2006).
24. L. Chávez-Gutiérrez, L. Bammens, I. Benilova, A. Vandersteen, M. Benurwar, M. Borgers, S. Lismont, L. Zhou, S. Van Cleynenbreugel, H. Esselmann, J. Wiltfang, L. Serneels, E. Karran, H. Gijsen, J. Schymkowitz, F. Rousseau, K. Broersen, B. De Strooper, The mechanism of γ-secretase dysfunction in familial Alzheimer disease. *EMBO J.* **31**, 2261–2274 (2012).
25. S. Kumar-Singh, J. Theuns, B. Van Broeck, D. Pirici, K. Vennekens, E. Corsmit, M. Cruts, B. Dermaut, R. Wang, C. Van Broeckhoven, Mean age-of-onset of familial Alzheimer disease caused by presenilin mutations correlates with both increased Aβ42 and decreased Aβ40. *Hum. Mutat.* **27**, 686–695 (2006).
26. J. J. Iliff, M. Wang, Y. Liao, B. A. Plogg, W. Peng, G. A. Gundersen, H. Benveniste, G. E. Vates, R. Deane, S. A. Goldman, E. A. Nagelhus, M. Nedergaard, A paravascular pathway facilitates CSF flow through the brain parenchyma and the clearance of interstitial solutes, including amyloid β. *Sci. Transl. Med.* **4**, 147ra111 (2012).
27. J. R. Cirrito, P. C. May, M. A. O'Dell, J. W. Taylor, M. Parsadanian, J. W. Cramer, J. E. Audia, J. S. Nissen, K. R. Bales, S. M. Paul, R. B. DeMattos, D. M. Holtzman, In vivo assessment of brain interstitial fluid with microdialysis reveals plaque-associated changes in amyloid-β metabolism and half-life. *J. Neurosci.* **23**, 8844–8853 (2003).
28. S. Hong, O. Quintero-Monzon, B. L. Ostaszewski, D. R. Podlisny, W. T. Cavanaugh, T. Yang, D. M. Holtzman, J. R. Cirrito, D. J. Selkoe, Dynamic analysis of amyloid β-protein in behaving mice reveals opposing changes in ISF versus parenchymal Aβ during age-related plaque formation. *J. Neurosci.* **31**, 15861–15869 (2011).
29. T. Iwatsubo, A. Odaka, N. Suzuki, H. Mizusawa, N. Nukina, Y. Ihara, Visualization of Aβ42(43) and Aβ40 in senile plaques with end-specific A β monoclonals: Evidence that an initially deposited species is A β 42(43). *Neuron* **13**, 45–53 (1994).
30. T. Grimmer, M. Riemenschneider, H. Förstl, G. Henriksen, W. E. Klunk, C. A. Mathis, T. Shiga, H. J. Wester, A. Kurz, A. Drzezga, Beta amyloid in Alzheimer's disease: Increased deposition in brain is reflected in reduced concentration in cerebrospinal fluid. *Biol. Psychiatry* **65**, 927–934 (2009).
31. M. P. Lambert, A. K. Barlow, B. A. Chromy, C. Edwards, R. Freed, M. Liosatos, T. E. Morgan, I. Rozovsky, B. Trommer, K. L. Viola, P. Wals, C. Zhang, C. E. Finch, G. A. Krafft, W. L. Klein, Diffusible, nonfibrillar ligands derived from $A\beta_{1-42}$ are potent central nervous system neurotoxins. *Proc. Natl. Acad. Sci. U.S.A.* **95**, 6448–6453 (1998).
32. R. Kayed, E. Head, J. L. Thompson, T. M. McIntire, S. C. Milton, C. W. Cotman, C. G. Glabe, Common structure of soluble amyloid oligomers implies common mechanism of pathogenesis. *Science* **300**, 486–489 (2003).
33. W. P. Esler, E. R. Stimson, J. M. Jennings, H. V. Vinters, J. R. Ghilardi, J. P. Lee, P. W. Mantyh, J. E. Maggio, Alzheimer's disease amyloid propagation by a template-dependent dock-lock mechanism. *Biochemistry* **39**, 6288–6295 (2000).
34. T. P. J. Knowles, C. A. Waudby, G. L. Devlin, S. I. A. Cohen, A. Aguzzi, M. Vendruscolo, E. M. Terentjev, M. E. Welland, C. M. Dobson, An analytical solution to the kinetics of breakable filament assembly. *Science* **326**, 1533–1537 (2009).
35. D. L. Elbert, B. W. Patterson, L. Ercole, V. Ovod, T. Kasten, K. Mawuenyega, K. Yarasheski, J. C. Morris, T. Benzinger, D. M. Holtzman, R. J. Bateman, Reply to: Fractional synthesis and clearance rates for amyloid β. *Nat. Med.* **17**, 1178–1179 (2011).
36. Y. Huang, R. Potter, W. Sigurdson, A. Santacruz, S. Shih, Y. E. Ju, T. Kasten, J. C. Morris, M. Mintun, S. Duntley, R. J. Bateman, Effects of age and amyloid deposition on Aβ dynamics in the human central nervous system. *Arch. Neurol.* **69**, 51–58 (2011).
37. J. H. Roh, Y. Huang, A. W. Bero, T. Kasten, F. R. Stewart, R. J. Bateman, D. M. Holtzman, Disruption of the sleep-wake cycle and diurnal fluctuation of β-amyloid in mice with Alzheimer's disease pathology. *Sci. Transl. Med.* **4**, 150ra122 (2012).
38. E. M. Reiman, Y. T. Quiroz, A. S. Fleisher, K. Chen, C. Velez-Pardo, M. Jimenez-Del-Rio, A. M. Fagan, A. R. Shah, S. Alvarez, A. Arbelaez, M. Giraldo, N. Acosta-Baena, R. A. Sperling, B. Dickerson, C. E. Stern, V. Tirado, C. Munoz, R. A. Reiman, M. J. Huentelman, G. E. Alexander, J. B. S. Langbaum, K. S. Kosik, P. N. Tariot, F. Lopera, Brain imaging and fluid biomarker analysis in young adults at genetic risk for autosomal dominant Alzheimer's disease in the presenilin 1 E280A kindred: A case-control study. *Lancet Neurol.* **11**, 1048–1056 (2012).
39. J. D. Harper, P. T. Lansbury Jr., Models of amyloid seeding in Alzheimer's disease and scrapie: Mechanistic truths and physiological consequences of the time-dependent solubility of amyloid proteins. *Annu. Rev. Biochem.* **66**, 385–407 (1997).
40. C. Cruchaga, S. Chakraverty, K. Mayo, F. L. Vallania, R. D. Mitra, K. Faber, J. Williamson, T. Bird, R. Diaz-Arrastia, T. M. Foroud, B. F. Boeve, N. R. Graff-Radford, P. St Jean, M. Lawson, M. G. Ehm, R. Mayeux, A. M. Goate; NIA-LOAD/NCRAD Family Study Consortium, Rare variants in *APP*, *PSEN1* and *PSEN2* increase risk for AD in late-onset Alzheimer's disease families. *PLoS One* **7**, e31039 (2012).
41. R. J. Bateman, L. Y. Munsell, J. C. Morris, R. Swarm, K. E. Yarasheski, D. M. Holtzman, Human amyloid-β synthesis and clearance rates as measured in cerebrospinal fluid in vivo. *Nat. Med.* **12**, 856–861 (2006).
42. D. N. Reeds, W. T. Cade, B. W. Patterson, W. G. Powderly, S. Klein, K. E. Yarasheski, Whole-body proteolysis rate is elevated in HIV-associated insulin resistance. *Diabetes* **55**, 2849–2855 (2006).
43. J. J. Cook, K. R. Wildsmith, D. B. Gilberto, M. A. Holahan, G. G. Kinney, P. D. Mathers, M. S. Michener, E. A. Price, M. S. Shearman, A. J. Simon, J. X. Wang, G. Wu, K. E. Yarasheski, R. J. Bateman, Acute γ-secretase inhibition of nonhuman primate CNS shifts amyloid precursor protein (APP) metabolism from amyloid-β production to alternative APP fragments without amyloid-β rebound. *J. Neurosci.* **30**, 6743–6750 (2010).
44. M. J. Savage, S. P. Trusko, D. S. Howland, L. R. Pinsker, S. Mistretta, A. G. Reaume, B. D. Greenberg, R. Siman, R. W. Scott, Turnover of amyloid β-protein in mouse brain and acute reduction of its level by phorbol ester. *J. Neurosci.* **18**, 1743–1752 (1998).

Acknowledgments: We thank the participants and their families for their contributions to this study and the Clinical Core of the Adult Children Study for clinical assessments of the participants. **Funding:** This work was supported by funding from the National Institute on Aging as a supplement, the Familial Adult Children Study (5P01AG026276-S1 to R.J.B.), to the Antecedent Biomarkers in AD: The Adult Children Study (5P01 AG026272 to J.C.M.). Additional support came from R01-NS065667 (R.J.B.), UL1 RR024992, P41 GM103422, P30 DK056341 (Nutrition Obesity Research Center, B.W.P.), P60 DK020579, and an anonymous foundation. **Author contributions:** R.J.B. designed the study and obtained funding. D.M.H., A.G., and J.C.M. assisted in the design of the study. W.S., R.J.B., and R.P. recruited and enrolled participants and performed tracer infusion studies. R.P., R.C., and T.K. performed laboratory protocol development, sample preparation, and processing. K.M. and V.O. developed MS methods, and V.O. measured samples by MS. B.W.P. and D.L.E. developed and performed kinetic modeling and statistical analyses. R.C. and K.E.Y. analyzed leucine samples. T.B., T.L.S.B., R.J.B., D.L.E., and B.W.P. developed images and videos. R.J.B. and R.P. wrote an initial draft of the paper. The final paper was prepared by B.W.P., D.L.E., and R.J.B., which all authors reviewed and approved. **Competing interests:** R.J.B. and D.M.H. are co-inventors on U.S. Patent 7,892,845 "Methods for measuring the metabolism of neurally derived biomolecules in vivo." Washington University, with R.J.B. and D.M.H. as co-inventors, has also submitted the U.S. nonprovisional patent application "Methods for measuring the metabolism of CNS derived biomolecules in vivo," serial #12/267,974. R.J.B., D.L.E., and B.W.P. are co-inventors on U.S. Provisional Application 61/728,692 "Methods of diagnosing amyloid pathologies using analysis of amyloid-beta enrichment kinetics." R.J.B. has consulted for Pfizer, DZNE, Probiodrug AG, Medscape, and EnVivo (SAB) and has research grants with AstraZeneca, Merck, and Eli Lilly in the past year. Washington University, R.J.B., and D.M.H. have a financial interest in C2N Diagnostics, which uses the SILK methodology in human studies. B.W.P. provides turnover kinetics consultation services for C2N Diagnostics. C2N Diagnostics did not support this work. D.M.H. has consulted for Pfizer, AstraZeneca, and Bristol-Myers Squibb in the last 12 months. His laboratory has received grants from Eli Lilly, AstraZeneca, Pfizer, and C2N Diagnostics that are not related to the content in this manuscript. T.B. has served on an advisory board for Eli Lilly and has received research funding from Avid Radiopharmaceuticals. These relationships are not related to the content in the manuscript. A.G. has received research funding during the last 12 months from Pfizer, Genentech, AstraZeneca, and iPierian and has served as a consultant for Amgen. These relationships are not related to the content in the manuscript. J.C.M. serves on scientific advisory boards for Eisai, Esteve, Janssen Alzheimer Immunotherapy Program, GlaxoSmithKline, Novartis, and Pfizer. The other authors declare that they have no competing interests.

Submitted 31 December 2012
Accepted 24 May 2013
Published 12 June 2013
10.1126/scitranslmed.3005615

Citation: R. Potter, B. W. Patterson, D. L. Elbert, V. Ovod, T. Kasten, W. Sigurdson, K. Mawuenyega, T. Blazey, A. Goate, R. Chott, K. E. Yarasheski, D. M. Holtzman, J. C. Morris, T. L. S. Benzinger, R. J. Bateman, Increased in vivo amyloid-β42 production, exchange, and loss in presenilin mutation carriers. *Sci. Transl. Med.* **5**, 189ra77 (2013).